Current Optics and Photonics
Vol. 2, No. 3, June 2018, pp. 233-240

ISSN: 2508-7266(Print) / ISSN: 2508-7274(Online)
DOI: https://doi.org/10.3807/COPP.2018.2.3.233

Two-mode Fiber with a Reduced Mode Overlap for Uncoupled Mode-division Multiplexing in C+L Band

Seongjin Hong[1], Kyoungyeon Choi[2], Yong Soo Lee[1], and Kyunghwan Oh[1]*

[1]Physics and Applied Physics, Yonsei University, Seoul 03722, Korea
[2]Department of Mechanical Engineering, Seoul National University, Seoul 03722, Korea

(Received February 20, 2018 : revised June 7, 2018 : accepted June 7, 2018)

We proposed a two-mode fiber (TMF) design that can effectively reduce the mode overlap between LP_{01} and LP_{11} modes by using a W-shaped index profile core structure, which is a primary concern in uncoupled mode division multiplexing (MDM). TMF has a three-layered core structure; central circular core, inner cladding, and outer ring core. We confirmed that in an optimal structure the LP_{01} mode was highly confined to the central core while the LP_{11} mode was guided along the outer ring core to result in a minimum overlap integral. We used a full-vectorial finite element method to estimate effective index, differential group delay (DGD), confinement loss, chromatic dispersion, and mode overlap controlling the parameters of the W-shaped structure. The optimized W-profile fiber provided optical characteristics within the ITU-T recommended standards over the entire C+L band.

Keywords : Optical fiber communication, Mode-division multiplexing, Two-mode fiber
OCIS codes : (060.0060) Fiber optics and optical communications; (060.4510) Optical communication; (230.7370) Waveguides

I. INTRODUCTION

Rapid data traffic increase along a conventional single mode fiber (SMF) communication network quickly exhausts the current fiber optic transmission capacity and various methods are being intensively investigated to accommodate the data increase [1-3]. Among these methods, mode division multiplexing (MDM) based on few-mode fibers (FMFs) has recently been reported by major telecom research laboratories and fiber manufacturers [4-6]. In contrast to multi-core fibers for space division multiplexing [7], the MDM based on FMF can be a practical solution to increase the transmission capacity, because of low connection loss between FMF and SMFs, mass production capability for FMFs, and relatively easier solutions for optical amplification along FMFs.

MDM is utilizing individual orthogonal modes in FMF as separate carriers and there have been two contrasting methods experimentally demonstrated. In the first method [8, 9], the mode coupling among the modes is compensated by electronically using multiple input multiple output (MIMO) processing at the receiver. The other method [10, 11] minimizes the mode coupling along FMF in order to optically separate each mode at the receiver.

Therefore, FMF structure should be optimized depending on its usage, and especially the coupling or cross talk between the propagating modes would be very contrasting issue in FMF design. In addition to the general requirements for such as low attenuation, large effective area, and a low bending loss, FMFs should have either a low DGD, or a low coupling between the adjacent modes [4, 5]. Low DGD is required in the first MDM method to reduce the signal processing burden in MIMO. On the while, low mode coupling between the modes is a mandatory requirement in the second MDM method and this might also reduce MIMO processing burden in the first method.

In the meantime, overall chromatic dispersion should be optimized to enable dense wavelength division multiplexing

*Corresponding author: koh@yonsei.ac.kr, ORCID 0000-0003-2544-0216
Color versions of one or more of the figures in this paper are available online.

(DWDM) even in FMF. In order to meet the requirements in both the low inter-symbol interference penalty and the low four-wave mixing impairments in DWDM, non-zero dispersion shifted fiber (NZDSF) has been developed and being widely used in long-haul applications, where the dispersion value within the transmission band was maintained at a non-zero low value [12]. Despite of its importance, non-zero dispersion value has not been fully addressed in prior FMF research.

In this study, we focus on FMF design for the uncoupled MDM, such that a new waveguide was designed to provide a minimum coupling along with a large effective index difference between two adjacent LP_{01} and LP_{11} modes. In order to achieve this goal we need to consider two key waveguide properties: the difference between the guided modes and their spatial mode overlap. It has been reported that the effective index difference (Δ_{neff}) between the adjacent propagation modes can play an important role in suppressing the crosstalk when Δ_{neff} is larger than $\sim 10^{-4}$ [13]. In the coupled mode theory [14], the overlap integral of two adjacent modes is known to be directly proportional to the mode coupling strength, and it should be minimized by optimal waveguide design. In order to use spatial filtering MDM at the receiver side, the overlap integral between LP_{01} and LP_{11} should be minimized for securing proper level of bit error rate [15, 16]. Despite the high importance in FMF design, detailed parametric analyses to reduce the overlap integral between the two modes have been very scarce in prior reports. Efforts to expand the operating spectral range of MDM to cover both C and L bands have been limited as well. We also optimized the chromatic dispersion of the two modes such that both of them satisfy the NZDSF requirements.

In this paper, a new TMF structure is proposed which is composed of the three-layered core; the central core, inner cladding layer, and the outer ring core as shown in Fig. 1 (a). This waveguide structure provides an efficient reduction of the modal overlap by confining the fundamental LP_{01} mode into the central core while separating it from the LP_{11} mode along the outer ring core as schematically shown in Fig. 1(b). Numerical modal analyses were performed by using full-vectorial finite element method (FEM) with the perfect matched layer (PML) boundary condition [17]. Optical properties of guided modes were optimized to satisfy ITU-T requirements in C+L band, for the first time to the best knowledge of the authors [18]. Relatively simple step index profile in the proposed waveguide could be easily mass-producible using the state of art fiber manufacturing technology and it can find practical applications in high capacity DMD.

II. PROPOSED WAVEGUIDE AND STRUCTURAL PARAMETERS

Cross section of the proposed two-mode fiber (TMF) is shown in Fig. 1(a). The inner cladding and outer cladding material is pure silica, whose optical dispersion was calculated using a Sellmeier equation for vitreous silica glass [19]. In reference to silica, the central core of radius a has an index difference Δn_1, whose optical property was calculated by using a Sellmeier equation for GeO_2 doped silica glass [20]. The outer ring core has the inner radius b, the outer radius c, and the index difference Δn_2. Δn_2 was also assumed to be raised by GeO_2 doping in silica. The inner cladding layer between the two cores acted as an optical barrier separating the two modes to reduce the modal overlap. The structural parameters of our TMF are summarized in Fig. 1(b).

By using vectorial FEM with the PML condition, the modal analyses were carried out for our TMF. The magnetic field propagating along the z-direction in the fiber can be expressed as:

$$\vec{H}(x,y,z,t) = \vec{H}(x,y)\exp[i(\omega t - \beta z)] \quad (1)$$

where β is the propagating constant and ω is the angular frequency. Eq. (2) shows an eigenvalue equation for magnetic field in the steady-state with a refractive index distribution, n.

$$\nabla \times (n^{-2}(\omega) \times \vec{H}) - k_0^2 \vec{H} = 0 \quad (2)$$

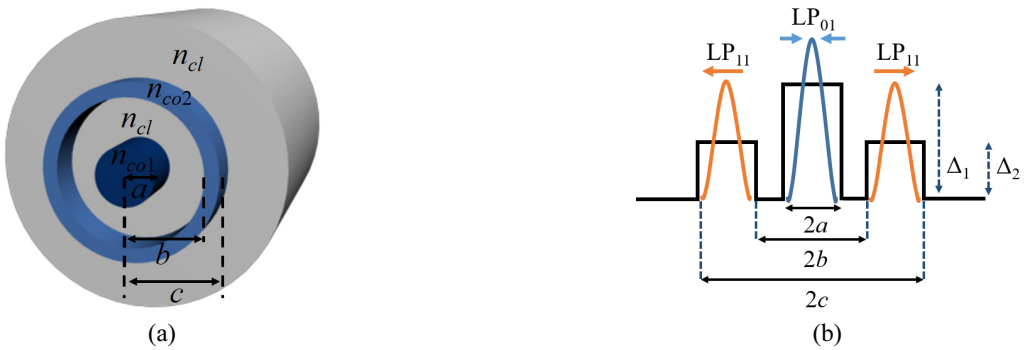

FIG. 1. Schematic cross section (a) and index profile (b) of proposed TMF.

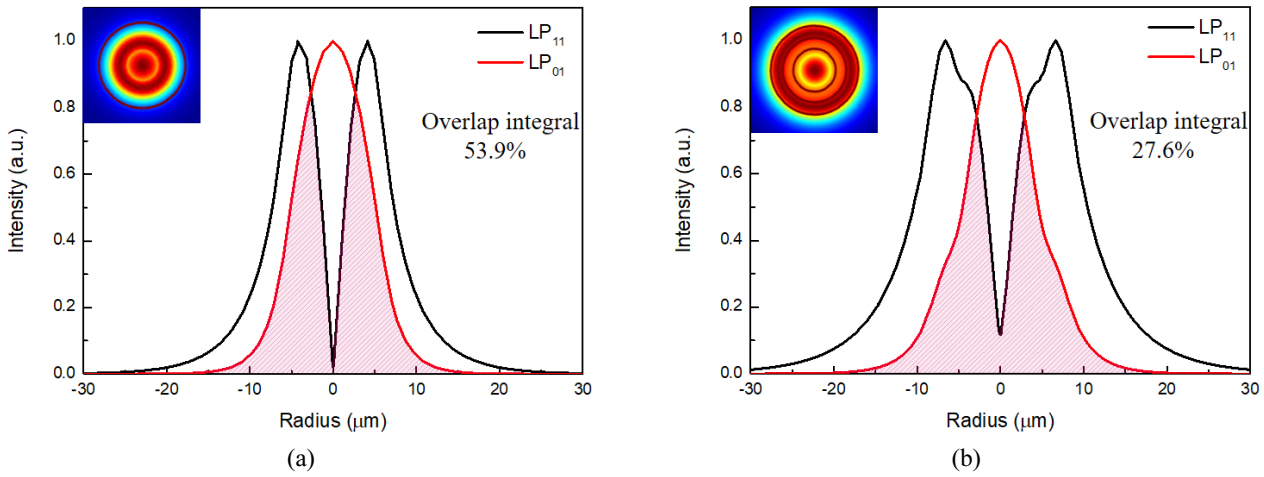

FIG. 2. Illustration of normalized mode power overlap of the LP_{01} and LP_{11} modes in single core TMF (a) and our designed TMF (b). Inset shows the transverse electrical fields of LP_{01}, and LP_{11}.

where k_0 is given by ω/c and c is the speed of light. The Sellmeier equation was used to evaluate wavelength dependent refractive index for silica cladding and GeO_2-doped silica core regions to account for correct material dispersion. By using FEM, Eq. (2) is solved with triangular meshes to find β. Subsequently the effective mode index n_{eff}, of the guided mode was obtained by taking the real part of β/k_0, while confinement loss was obtained from its imaginary part [21]. In the analysis, boundary conditions for the inner elements were set to satisfy the continuity conditions and the outer boundary was set to be continuous with the PML [21].

Figure 2 briefly describes the role of triple-layered core in reducing the overlap integral and subsequently the mode coupling between LP_{01} and LP_{11} modes, illustration of normalized mode power overlap of the LP_{01} and LP_{11} modes in single core TMF (a) and our designed TMF (b). Inset shows the transverse electrical fields of LP_{01}, and LP_{11}. Normalized modal intensity profiles at the wavelength of $\lambda = 1550$ nm are compared for (a) the single core step index fiber with the core radius of 6 μm and $\Delta n = 0.$ 36%. In Fig. 2(b), our TMF has the structural parameters: $a =$ 4.1 μm, $b = 6$ μm, $c = 8.2$ μm, $\Delta n_1 = 0.36\%$, and $\Delta n_2 =$ 0.31%. It is clearly shown that the spatial overlap between LP_{01} and LP_{11} modes is significantly reduced almost by a factor of two in our proposed TMF, which confirms the unique role of three-layered core to spatially separate the two modes LP_{01} and LP_{11}.

III. MODAL CHARACTERISTICS OF TMF

3.1. Two Mode LP_{01} and LP_{11} Guidance

In order to confirm that our proposed waveguide structure allows two-mode guidance we numerically calculated the effective indices of LP_{01}, LP_{11} and LP_{21} modes and investigated their cut-off behavior. In the calculations, we fixed parameters for the central core; $a = 4.1$ μm and $\Delta n_1 =$ 0.36%, which will allow a low connection loss with commercial SMF [22]. Figures 3 and 4 show effective mode index of each mode, LP_{01}, LP_{11}, and LP_{21}, as a function of waveguide parameters b, c, and Δn_2. We choose the wavelength 1530 and 1625 nm, the shortest wavelength of the C-band and the longest wavelength of the L-band [23]. If the two-mode condition is satisfied at these two wavelengths, it would be valid in the entire wavelength in C+L band. As shown in Figs. 3(a) and 4(a), the effective indices of the LP_{01}, and LP_{11} modes were found to be higher than the silica cladding index for the given ranges of b, c, and Δn_2, which ensured that the two modes are guided along the proposed TMF. Figs. 3(b) and 4(b) show the effective index of the LP_{21} mode and it should be lower than the silica cladding index to satisfy the two-mode guidance condition [20]. Based upon the modal guidance analyses in Figs. 3 and 4, we obtained the reference structural parameters $a = 4.1$ μm, $b = 6$ μm, $c =$ 8.2 μm, $\Delta n_1 = 0.36\%$, and $\Delta n_2 = 0.31\%$ satisfying the two-mode condition and they are summarized in Table 1.

3.2. Effective Index Difference between the LP_{01} and LP_{11} Modes

It is wellknown that a large effective index difference Δn_{eff} between the adjacent propagation modes can suppress the mode coupling between propagated modes [26]. One of previous works [13] has shown that Δn_{eff} larger than $\sim 10^{-4}$ can efficiently suppress the crosstalk between the modes. Figure 5(a) shows the effective indices of the LP_{01}, and LP_{11} modes. In the optimized TMF design, we obtained a large effective index difference between LP_{01} and LP_{11} with $\Delta n_{eff} = \sim 2 \times 10^{-3}$ in the entire C+L band, which is an order of magnitude larger than the required value. In addition, Fig. 5(b) shows that effective index of the LP_{21} mode in the given parameters of Table 1, which confirmed that this mode was not guided in our TMF.

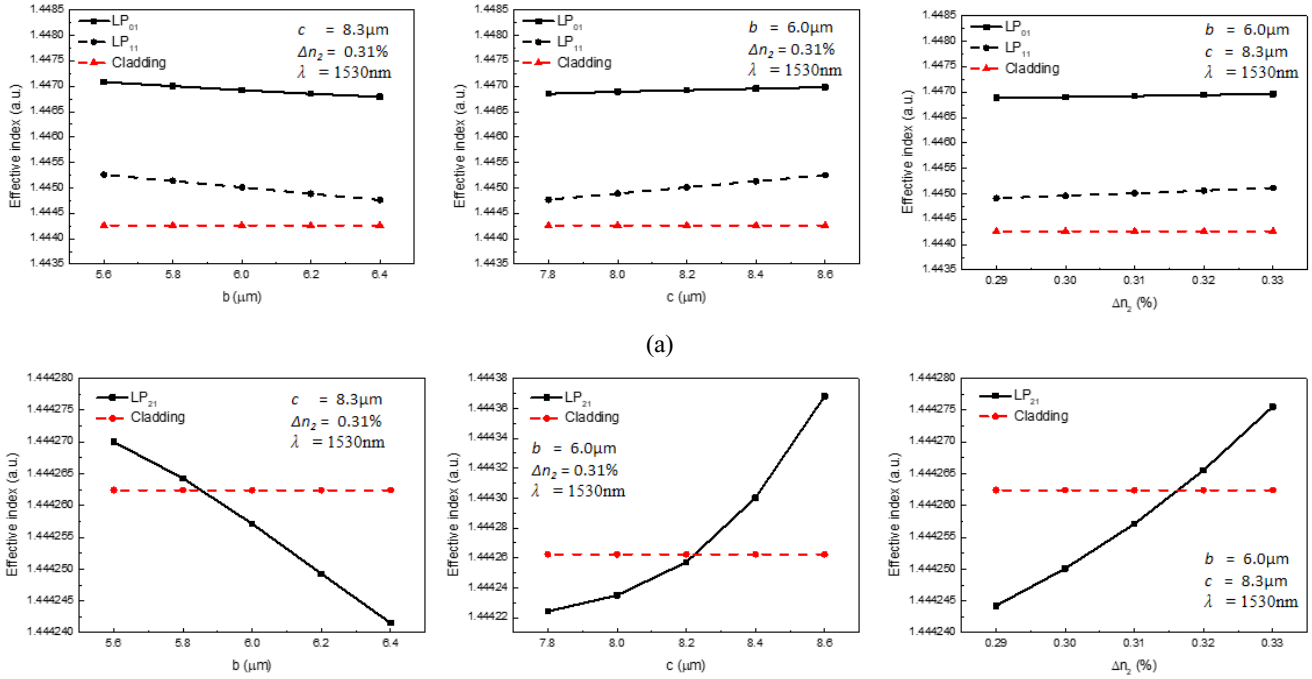

FIG. 3. Variation of the effective index of (a) LP_{01}, and LP_{11} modes (b) LP_{21} as a function of b, c, and Δn_2 at 1530 nm the shortest wavelength of C-band. Here we set a = 4.1 μm, b = 6 μm, c = 8.2 μm, Δn_1 = 0.36%, and Δn_2 = 0.31%. Dashed red line indicates the silica cladding index and structural parameters are set for n_{eff} of LP_{21} is located below the dashed line. This means that the LP_{21} mode is not guided.

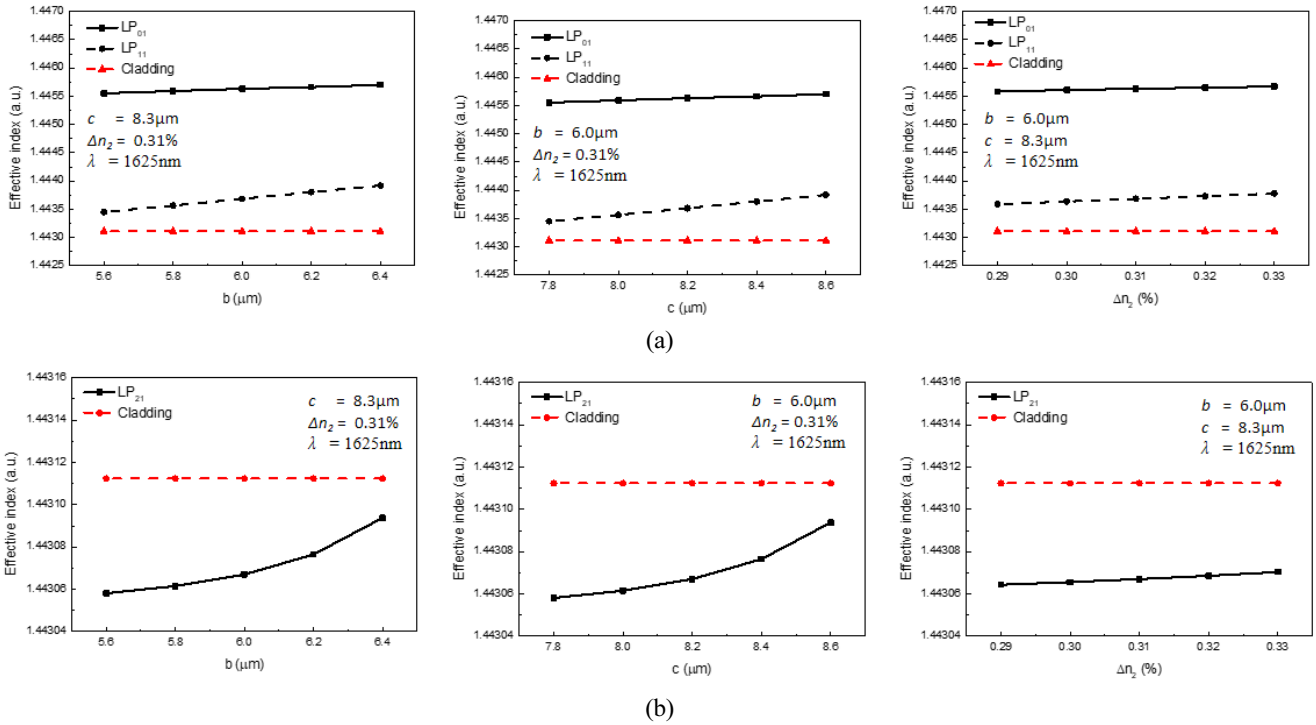

FIG. 4. Variation of the effective index of (a) LP_{01}, and LP_{11} modes (b) LP_{21} as a function of b, c, and Δn_2 at 1625 nm the longest wavelength of L-band. Here we set a = 4.1 μm, b = 6 μm, c = 8.2 μm, $\Delta n1$ = 0.36%, and Δn_2 = 0.31%. Dashed red line indicates the silica cladding index and it shows that two-mode conditions is satisfied.

TABLE 1. Optimized parameters of designed TMF

Structural parameter	Value
a	4.1 μm
b	6 μm
c	8.2 μm
Δn_1	0.36 %
Δn_2	0.31 %
Clad index (at 1.55 μm)	1.4440

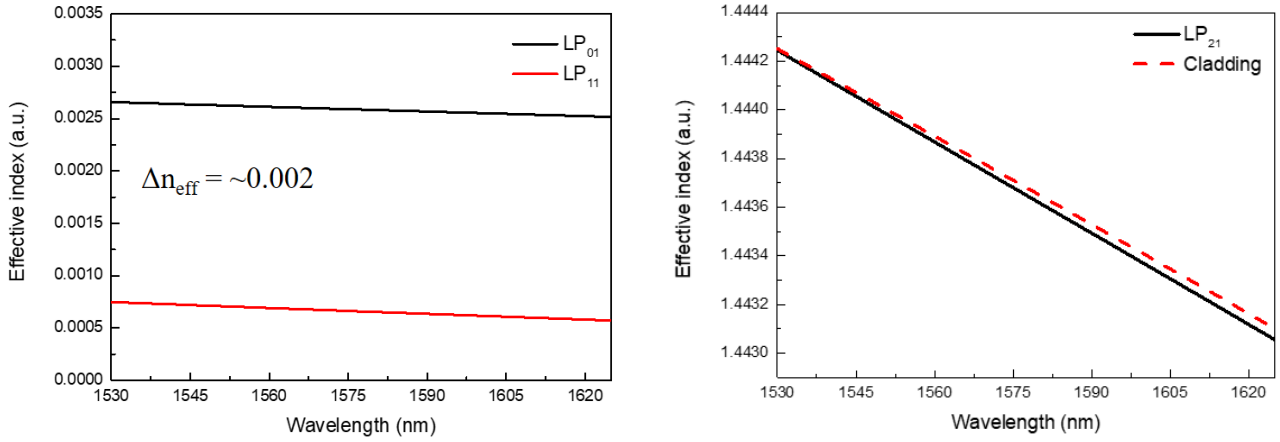

FIG. 5. Effective indices of (a) the LP_{01} and the LP_{11} mode and (b) the LP_{21} mode in C+L band. The LP_{21} mode index is lower than cladding index from 5×10^{-6} to 4.5×10^{-5}. This indicates that LP_{21} modes is not a guided mode in designed fiber.

3.3. Effective Mode Area

The effective mode area A_{eff} of the LP_{01} and LP_{11} modes was calculated using the following equation:

$$A_{eff} = \frac{(\int IdA)^2}{\int I^2 dA} \tag{3}$$

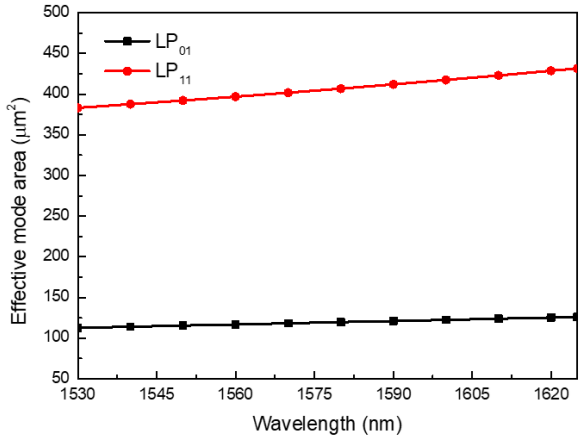

FIG. 6. Effective mode area of LP_{01} and LP_{11} modes in C+L wavelength range.

Figure 6 shows the A_{eff} of the LP_{01} and LP_{11} in our designed fiber. A_{eff} of the LP_{01} mode monotonically increased from 112 μm² to 126 μm² in the C+L band. A_{eff} of the LP_{11} increased from 383 μm² to 431 μm². It is noted that A_{eff} of the LP_{01} mode in our TMF was comparable to those of previous reports [27, 28], while A_{eff} of the LP_{11} mode in our TMF was larger by a factor of two. Large effective area in our TMF ensures reduction of nonlinear effects and high optical power capacity in MDM applications.

3.4. Mode Overlap Integral

The overlap integral between the LP_{01} and LP_{11} modes can be expressed as:

$$Overlap\ integral = \frac{\int \frac{I_{01}}{\int I_{01}dA} \times \frac{I_{11}}{\int I_{11}dA} dA}{\int (\frac{I_{01}}{\int I_{01}dA})^2 dA} \tag{4}$$

where I_{01}, and I_{11} are the intensities of the LP_{01} and LP_{11} modes, respectively. In this study we used the normalized mode intensities to investigate the mode coupling along TMF.

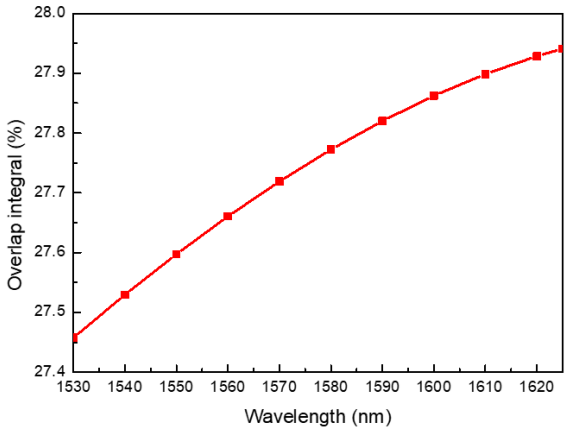

FIG. 7. Overlap integral between LP_{01} and LP_{11} modes over the C+L band spectral range.

In comparison to the single core step index fiber which has 53.9% overlap integral with the core radius of 6 μm and $\Delta n = 0.36\%$. The overlap integral of the proposed fiber is estimated about 27.6% at $\lambda = 1550$ nm, which corresponds to a half the single core step index fiber as shown in Fig. 2. We further investigated the change of the overlap integral in the C+L band and the results are summarized in Fig. 7. The overlap integral monotonically increased from 27.45% to 27.94%. This low overlap integral can efficiently suppress the mode coupling in our TMF providing less difficulty in separating guided modes at the receiver side [16].

3.5. Dispersion and Differential Group Delay Properties

Chromatic dispersion of the LP_{01} and LP_{11} modes in our TMF was calculated as a function of wavelength using the real part of n_{eff} and Eq. (5).

$$Dispersion = -\frac{\lambda}{c}\left(\frac{\partial^2 n_{eff}}{\partial \lambda^2}\right) \tag{5}$$

The results are summarized in Fig. 8. Both the LP_{01} and LP_{11} modes showed negative dispersion owing to the triple layered core structure. Their values were between 3.5 and 5.5 ps/km/nm over the entire C+L band. These chromatics dispersion values are suitable for NZDSF for dense wavelength division multiplexing (DWDM) fiber optical networks and satisfy the requirement of ITU-T NZDSF recommendations [29] for the chromatic dispersion range. Utilizing these properties, it is further applicable not only for MDM but also for WDM.

Low DGD is important for relaxing the complexity of MIMO processing [24]. We defined the DGD between LP_{01} and LP_{11} as follows:

$$DGD = \left(\frac{n_{eff,01} - n_{eff,11}}{c}\right) - \frac{\lambda}{c}\left(\frac{\partial n_{eff,01}}{\partial \lambda} - \frac{\partial n_{eff,11}}{\partial \lambda}\right) \tag{6}$$

where $n_{eff,01}$ and $n_{eff,11}$ is the effective index of the LP_{01}, and LP_{11} mode, respectively. Here c is the speed of light. In Fig. 8(b), DGD of our TMF is plotted over the C+L band and the value was about ~4 ps/m, which is very comparable to prior step-index few mode fibers [25].

3.6. Confinement Loss Estimation

In order to further confirm that the proposed TMF guides the two modes, we calculated the confinement loss α using full vector FEM analyses with PML condition in dB/km from the imaginary part of the propagation constant, β [21].

$$\alpha = 20\log_{10}(e)\cdot \mathrm{Im}(\beta) \tag{7}$$

In order to properly guide a mode along a fiber, the confinement loss should be lower than 10^{-4} dB/km in the spectral range of interest. Figure 9(a) shows the confinement loss of the LP_{01}, and the LP_{11} mode and it was lower than

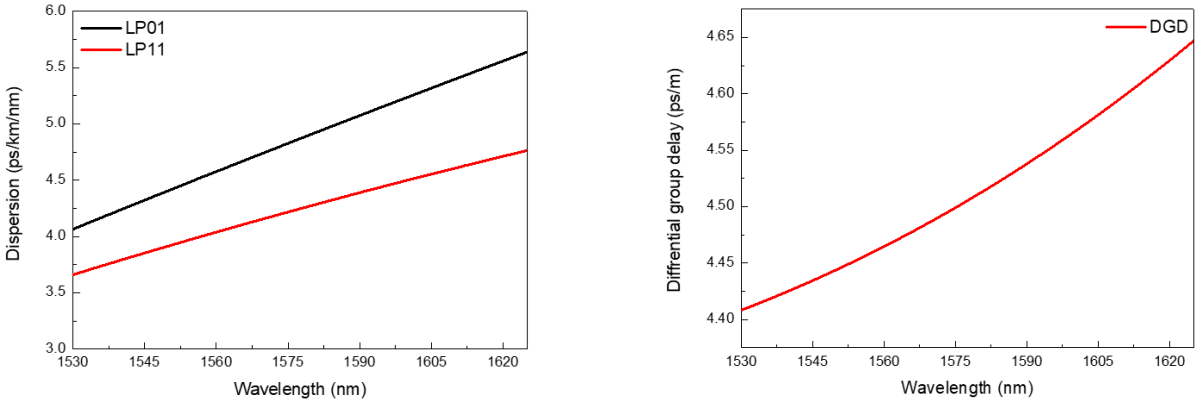

(a) (b)

FIG. 8. (a) Chromatic dispersion of the LP_{01} and the LP_{11} modes in C+L band spectral range. (b) Differential group delay between the LP_{01} and the LP_{11} modes in C+L band spectral range.

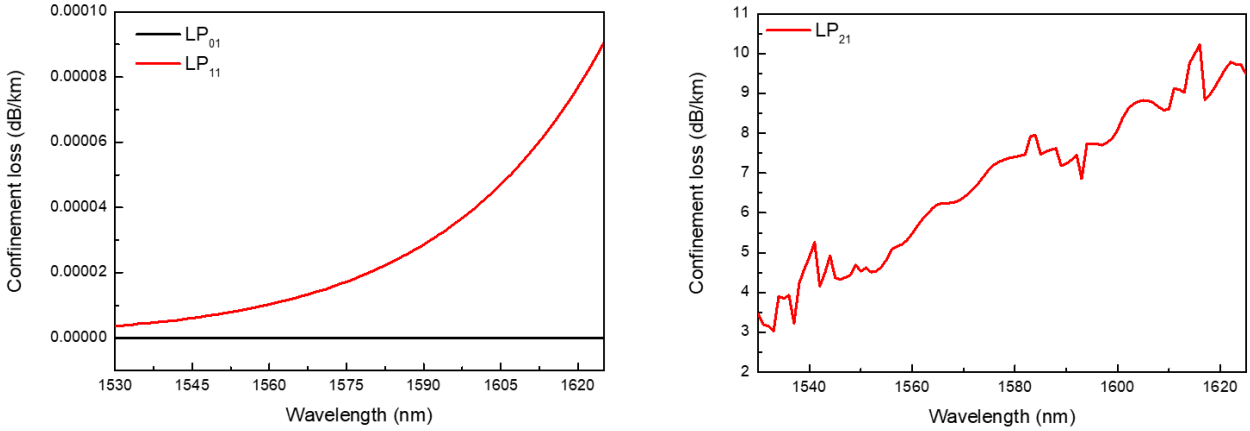

(a) (b)

FIG. 9. Confinement loss of (a) the LP_{01} and the LP_{11} modes and (b) the LP_{21} mode in the C+L band spectral range.

TABLE 2. Modal characteristics at 1550 nm for the designed TMF

Optical properties	Unit	Value
$n_{eff,\,01}$	-	1.44665
$n_{eff,\,11}$	-	1.44473
$n_{eff,\,01}$ - $n_{eff,\,11}$	-	1.9×10^{-3}
Overlap integral between LP_{01} and LP_{11}	%	27.6
DGD between LP_{01} and LP_{11}	ps/m	4.4
Dispersion LP_{01}	ps/km/nm	4.4
Dispersion LP_{11}	ps/km/nm	3.9
Effective area LP_{01}	μm^2	115.5
Effective area LP_{11}	μm^2	392.2
Confinement loss LP_{01}	dB/km	1.4×10^{-8}
Confinement loss LP_{11}	dB/km	7.2×10^{-6}

10^{-4} dB/km for both modes. We could confirm that our proposed TMF would provide sufficient guidance for both the LP_{01} and the LP_{11} modes. In contrast, the confinement loss of the LP_{21} was as large as few dB/km as shown in Fig. 9(b), which confirms that our TMF indeed guides only two modes, LP_{01} and LP_{11}.

IV. CONCLUSION

We have designed a new TMF for uncoupled MDM applications. Our proposed TMF waveguide was based on a three-layered core composed of a central core, an inner cladding, and an outer ring core. We successfully reduced the modal overlap by confining the LP_{01} mode to the central core and the LP_{11} mode to the outer ring core. Using a full vectorial finite element method, we optimized the TMF structural parameters so that it can guide the LP_{01} and the LP_{11} modes with a large effective index difference $\Delta n_{eff} = \sim 2 \times 10^{-3}$ in the entire C+L band spectral range, which is an order of magnitude larger than the normally required value. The proposed TMF provided a low modal overlap between the LP_{01} and the LP_{11} mode of less than 27.9%, which could be a strong indicator to suppress the modal coupling. Additionally, the proposed TMF showed a low DGD (4.4~4.6 ps/m), a large A_{eff} of the LP_{01} (112~126 μm^2) and LP_{11} (383~431 μm^2), and an appropriate chromatic dispersion (3.5~5.5 ps/km/nm) in Table 2, which confirmed the proposed waveguide structure is viable, and practical MDM applications.

ACKNOWLEDGMENT

This work was supported in part by ICT R&D Program of MSIP/IITP (2014-3-00524), in part by Nano Material Technology Development Program through NRF funded by the MSIP (NRF-2012M3A7B4049800), and in part by Basic Science Research Program through the National Research Foundation of Korea (NRF) funded by the

Ministry of Science, ICT & Future Planning (No. 2016k 1A3A1A09918616).

REFERENCES

1. L. Schares, B. G. Lee, F. Checconi, R. Budd, A. Rylyakov, N. Dupuis, F. Petrini, C. L. Schow, P. Fuentes, and O. Mattes, "A throughput-optimized optical network for data-intensive computing," IEEE Micro **34**, 52-63 (2014).
2. R.-J. Essiambre, G. Kramer, P. J. Winzer, G. J. Foschini, and B. Goebel, "Capacity limits of optical fiber networks," J. Lightw. Technol. **28**, 662-701 (2010).
3. L. Ma, K. Tsujikawa, N. Hanzawa, S. Aozasa, S. Nozoe, and F. Yamamoto, "Design and fabrication of low loss hole-assisted few-mode fibers with consideration of surface imperfection of air holes," J. Lightw. Technol. **34**, 5164-5169 (2016).
4. L. Grüner-Nielsen, Y. Sun, J. W. Nicholson, D. Jakobsen, K. G. Jespersen, R. Lingle Jr, and B. Pálsdóttir, "Few mode transmission fiber with low DGD, low mode coupling, and low loss," J. Lightw. Technol. **30**, 3693-3698 (2012).
5. P. Sillard, M. Bigot-Astruc, and D. Molin, "Few-mode fibers for mode-division-multiplexed systems," J. Lightw. Technol. **32**, 2824-2829 (2014).
6. K.-P. Ho and J. M. Kahn, "Mode coupling and its impact on spatially multiplexed systems," Opt. Fiber Telecommun. VI **17**, 1386-1392 (2013).
7. D. M. Marom and M. Blau, "Switching solutions for WDM-SDM optical networks," IEEE Commun. Mag. **53**, 60-68 (2015).
8. R. Ryf, S. Randel, A. H. Gnauck, C. Bolle, A. Sierra, S. Mumtaz, M. Esmaeelpour, E. C. Burrows, R.-J. Essiambre, and P. J. Winzer, "Mode-division multiplexing over 96 km of few-mode fiber using coherent 6 × 6 MIMO processing," J. Lightw. Technol. **30**, 521-531 (2012).
9. C. Koebele, M. Salsi, D. Sperti, P. Tran, P. Brindel, H. Mardoyan, S. Bigo, A. Boutin, F. Verluise, and P. Sillard, "Two mode transmission at 2 × 100 Gb/s, over 40 km-long prototype few-mode fiber, using LCOS-based programmable mode multiplexer and demultiplexer," Opt. Express **19**, 16593-16600 (2011).
10. N. Hanzawa, K. Saitoh, T. Sakamoto, T. Matsui, S. Tomita, and M. Koshiba, "Demonstration of mode-division multiplexing transmission over 10 km two-mode fiber with mode coupler," in *Proc. Optical Fiber Communication Conference* (Optical Society of America, 2011), p. OWA4.
11. P. Sillard, M. Astruc, D. Boivin, H. Maerten, and L. Provost, "Few-mode fiber for uncoupled mode-division multiplexing transmissions," in *Proc. European Conference and Exposition on Optical Communications* (Optical Society of America, 2011), p. Tu. 5. LeCervin. 7.
12. N. Kumano, K. Mukasa, M. Sakano, and H. Moridaira, "Development of a non-zero dispersion-shifted fiber with ultra-low dispersion slope," Furukawa Rev. **22**, 1-6 (2002).
13. N. Riesen, J. D. Love, and J. W. Arkwright, "Few-mode elliptical-core fiber data transmission," IEEE Photon. Technol. Lett. **24**, 344 (2012).
14. A. W. Snyder, "Coupled-mode theory for optical fibers," J. Opt. Soc. Am. **62**, 1267-1277 (1972).
15. K. Nakajima, P. Sillard, D. Richardson, M.-J. Li, R.-J. Essiambre, and S. Matsuo, "Transmission media for an SDM-based optical communication system," IEEE Commun. Mag. **53**, 44-51 (2015).
16. Y.-M. Jung, S.-U. Alam, and D. J. Richardson, "All-fiber spatial mode selective filter for compensating mode dependent loss in MDM transmission systems," in *Proc. Optical Fiber Communication Conference* (Optical Society of America, 2015), p. W2A. 13.
17. Y. S. Lee, C. G. Lee, Y. Jung, M.-K. Oh, and S. Kim, "Highly birefringent and dispersion compensating photonic crystal fiber based on double line defect core," J. Opt. Soc. Korea **20**, 567-574 (2016).
18. Characteristics of a Cut-Off Shifted, Single-Mode Fibre and Cable, ITU-T Std. G.654, Oct. (2012).
19. B. Brixner, "Refractive-index interpolation for fused silica," J. Opt. Soc. Am. **57**, 674-676 (1967).
20. K. Oh and U.-C. Paek, *Silica optical fiber technology for devices and components: design, fabrication, and international standards* (John Wiley & Sons, 2012).
21. M. Park, H. E. Arabi, S. Lee, and K. Oh, "Independent control of birefringence and chromatic dispersion in a photonic crystal fiber using two hollow ring defects," Opt. Commun. **284**, 4914-4919 (2011).
22. Corning, "Corning SMF-28 optical fiber product information," http://ece466.groups.et.byu.net/notes/smf28.pdf.
23. O. Bands, B. Laurent, and G. Draka, "From O to L: The future of optical-wavelength bands," Broadband Properties, 83-85 (2008).
24. F. Ferreira, D. Fonseca, and H. Silva, "Design of few-mode fibers with arbitrary and flattened differential mode delay," IEEE Photon. Technol. Lett. **25**, 438-441 (2013).
25. M. Kasahara, K. Saitoh, T. Sakamoto, N. Hanzawa, T. Matsui, K. Tsujikawa, and F. Yamamoto, "Design of three-spatial-mode ring-core fiber," J. Lightw. Technol. **32**, 1337-1343 (2014).
26. J. Zhao, M. Tang, K. Oh, Z. Feng, C. Zhao, R. Liao, S. Fu, P. P. Shum, and D. Liu, "Polarization-maintaining few mode fiber composed of a central circular-hole and an elliptical-ring core," Photon. Res. **5**, 261-266 (2017).
27. M. Bigot-Astruc, L. Provost, G. Krabshuis, P. Dhenry, and P. Sillard, "125 μm glass diameter single-mode fiber with Aeff of 155 μm 2," in *Proc. Optical Fiber Communication Conference* (Optical Society of America, 2011), p. OTuJ2.
28. K. Takenaga, Y. Sasaki, N. Guan, S. Matsuo, M. Kasahara, K. Saitoh, and M. Koshiba, "Large effective-area few-mode multicore fiber," IEEE Photon. Technol. Lett. **24**, 1941-1944 (2012).
29. Characteristics of a non-zero dispersion-shifted single-mode optical fibre and cable, ITU-T G.655, Nov. (2009).